



# Leaf hyperspectral reflectance as a potential tool to detect diseases associated with vineyard decline

Amanda Heemann Junges<sup>1</sup> · Marcus André Kurtz Almança<sup>2</sup> · Thor Vinícius Martins Fajardo<sup>3</sup> · Jorge Ricardo Ducati<sup>4</sup>

Received: 8 November 2019 / Accepted: 17 July 2020 / Published online: 11 August 2020  
© Sociedade Brasileira de Fitopatologia 2020

## Abstract

Grape production in the Serra Gaúcha region, south of Brazil, is severely constrained by several diseases such as the decline and death syndrome caused grapevine trunk (fungal) diseases (GTDs) and the grapevine leafroll-associated virus (*GLRaV*). As pathogens induce changes in leaf tissue that modify the reflectance, the spectral signature of asymptomatic and symptomatic grapevine leaves infected by GTDs and *GLRaV* was analyzed to check whether spectral responses could be useful for disease identification. This work aims at (a) defining the spectral signature of grapevine leaves asymptomatic and symptomatic to GTDs and *GLRaV*; b) analyzing whether the spectral response of asymptomatic leaves can be distinguished from symptomatic; and (c) defining the most useful wavelengths for discriminating spectral responses. For such, reflectance of leaves in either condition collected in a “Merlot” vineyard during three growing seasons was measured using a spectroradiometer. Principal components and partial least square discriminant analyses confirmed the spectral separation and classes discrimination. The average spectra, difference spectra, and first-order derivative (FOD) spectra indicated differences between asymptomatic and symptomatic leaves in the green peak (520–550 nm), chlorophyll-associated wavelengths (650–670 nm), red edge (700–720 nm), beginning of near-infrared (800–900 nm), and shortwave infrared. Hyperspectral data was linked to biochemical and physiological changes described for GTD and *GLRaV*. Variable importance in the projection (VIP) analysis showed that some wavelengths allowed to differentiate the tested pathosystems and could serve as a basis for further validation and disease classification studies.

**Keywords** Grapevine leafroll-associated virus · Grapevine trunk diseases · *Vitis vinifera* L. · Principal components analysis · Variable importance in the projection

---

**Electronic supplementary material** The online version of this article (<https://doi.org/10.1007/s40858-020-00387-0>) contains supplementary material, which is available to authorized users.

---

✉ Amanda Heemann Junges  
amandahj@hotmail.com

- <sup>1</sup> Departamento de Diagnóstico e Pesquisa Agropecuária, Secretaria da Agricultura, Pecuária e Desenvolvimento Rural, Veranópolis, RS 95330-000, Brazil
- <sup>2</sup> Campus Bento Gonçalves Instituto Federal de Educação, Ciência e Tecnologia do Rio Grande do Sul, Bento Gonçalves, RS 95700-206, Brazil
- <sup>3</sup> Embrapa Uva e Vinho, Bento Gonçalves, Rio Grande do Sul 95701-008, Brazil
- <sup>4</sup> Universidade Federal do Rio Grande do Sul, Instituto de Física Departamento de Astronomia, Porto Alegre, RS 91501-970, Brazil

## Introduction

Brazil ranks fifth in wine production in the Southern Hemisphere. The Serra Gaúcha region, the most important wine-producing area in the country, accounts for 85% of the national wine production (Ibravin 2019). In this region, one of the biggest obstacles for producing high-quality grape is the decline and death of plants in vineyards caused by a complex of agents often associated with fungal and viral diseases (Basso et al. 2017).

Grapevine trunk diseases (GTDs) are especially important because of the economic losses that result from branch death that reduces grape yields, increased costs for controlling the disease, and reduced vineyard life (Gramaje et al. 2018). The GTD complex includes Petri disease and Esca disease complex (*Phaeoconiella chlamydospora*, *Phaeoacremonium* spp., and *Fomitiporia* spp.), black dead arm (*Botryosphaeria* spp. and other fungi of the *Botryosphaeriaceae* family), *Eutypa* dieback (*Eutypa* spp.), and black foot (*Cylindrocarpon* spp., *Ilyonectria*

spp., *Campylocarpon* spp.) (Úrbez-Torres et al. 2014; Silva et al. 2017). The fungi associated with GTDs in the Serra Gaúcha region have reported in previous studies (Garrido et al. 2004; Almança et al. 2013).

Among the viral diseases, the grapevine leafroll disease (GLD) is caused by some viruses known as grapevine leafroll-associated virus (GLRaV) of the Closteroviridae family, of which the GLRaV-3 is the most prevalent and widespread (Naidu et al. 2014, 2015). GLRaV is an economically important disease that occurs in most grape-growing regions worldwide (Mac Donald et al. 2016). The economic losses result from the reduced photosynthetic activity leads to lower fruit quality, reduced yield, and vine decline (Basso et al. 2017).

Many vineyards show mixed infections by GTDs and GLRaV, making it challenging to inspect visually all acreage within the optimal period for disease expression (Mac Donald et al. 2016). The photosynthetic process and the plant tissue cell structures attacked by pathogens suffer alterations that modify the vegetation and electromagnetic radiation interaction and, consequently, leaf and canopy reflectances in the visible (VIS), near-infrared (NIR), and shortwave infrared wavelengths (SWIR) (Prabhakar et al. 2012; Calcante et al. 2012; Martinelli et al. 2015; Mahlein 2016; Heim et al. 2018; Zarco-Tejada et al. 2018; Gold et al. 2019, 2020; Fallon et al. 2020). Light reflection in the VIS, NIR, and SWIR provides a comprehensive assessment of plant responses to diseases due to changing in biochemical (e.g., leaf pigments, nutrient composition, and secondary metabolism) and physiological (e.g., photosynthetic activity and water) aspects (Couture et al. 2018). Therefore, plant spectral properties can assist in the development of stress signatures for diseases. In fact, there is a growing interest in using spectral reflectance measurements to detect and discriminate among plant diseases (Mahlein 2016).

Recent developments in various pathosystems using different sensors have shown changes in the spectral behavior associated with grapevine diseases. For viruses, Naidu et al. (2009) reported differences in leaf hyperspectral reflectance of two red-berried wine grape cultivars with and without the presence of GLRaV-3. For fungal diseases, changes in the spectral reflectance were reported by several authors: Calcante et al. (2012) examining “Cabernet Franc” leaves with downy mildew (*Plasmopara viticola*) infection; Knauer et al. (2017) and Pérez-Roncal et al. (2020) studying powdery mildew (*Erysiphe necator*) infection levels in “Chardonnay” and “Carignan Noir” grape bunches; Oerke et al. (2016) to differentiate grapevine cultivars with distinctive resistance to *P. viticola*; Di Gennaro et al. (2016) to GTD’s symptoms in “Cabernet Sauvignon” vineyard; and Junges et al. (2018) to GTD’s (Esca Complex) symptoms in “Merlot” leaves. These studies have confirmed the distinct spectral behavior of asymptomatic leaves (or canopies) compared to leaves

symptomatic to a specific causal agent and focusing on the binary discrimination between healthy and diseased plants. Mahlein et al. (2010) showed specific spectral signatures for three fungal leaf diseases of sugar beet, suggesting that the diseases had a differential effect on the reflectance, thus showing the potential of integrating remote sensing methods for disease detection.

It is noteworthy that the spectral reflectance signatures should be specific to the effects of a plant-pathogen interaction and then research is required to more fully explore the potential of this technique for a range of pathosystems and crop production systems (Heim et al. 2018). In the vineyears of the Serra Gaúcha, the most common scenario is the co-occurrence of plants with GTDs and GLRaV symptoms leading to plant decline, for which no spectral signature data are available for such situation. The use hyperspectral data to detect crop diseases is a promising and novel approach for classifying disease status as well as for nondestructive assessment of specific responses of the plant to disease infection (Couture et al. 2018; Zarco-Tejada et al. 2018; Fallon et al. 2020). In this study, we hypothesized that (1) leaves infected by fungal or viral disease symptoms associated with vine decline show a distinct spectral behavior in comparison with asymptomatic leaves; (2) the hyperspectral reflectance changes in symptomatic leaves is linked to biophysical or biochemical characteristics associated with the specific pathogen infection; (3) it is necessary to reduce the high dimensionality of hyperspectral data defining the important wavelengths for diseases differentiation. The objective of this work was to define the spectral signature and the most useful wavelengths for discriminating grapevine leaves separated into categories asymptomatic (1), GLRaV symptoms (2), GTDs initial (3), and advanced (4) symptoms.

## Material and methods

### Site, crop, and disease characterization

The study area consisted of a commercial vineyard (cultivar Merlot) in Veranópolis, in the Serra Gaúcha region, Rio Grande do Sul, Brazil. According to Köppen classification (Alvares et al. 2013), the regional climate is Cfb: *C* indicates temperate climate, *f* is humid, without a dry season with monthly average rainfall no less than 60 mm, and *b* indicates average air temperature below 22 °C in the hottest month.

In Veranópolis, the 1956–2015 data series shows 1683 mm annual average rainfall with a 140 mm monthly average, ranging from 109 mm in May to 181 mm in September (Junges et al. 2019). The annual average temperature is 17.3 °C, ranging from 12.7 °C (July) to 21.8 °C (January) (Junges 2018). The north-south oriented “Merlot” vineyard is conducted in

the vertical training system and was studied during all vegetative seasons since 2015 (2015/2016 to 2018/2019).

The plants exhibited GTDs and GLRaV symptoms whereas the presence of pathogens was confirmed in the lab. The GTDs laboratory diagnosis consisted of isolating the fungi in PDA (potato-dextrose-agar) culture medium from plant samples with vascular internal symptoms, as described by Almança et al. (2013). GTDs were diagnosed by evaluating the internal symptoms and morphological characterization of the colony and spores of the isolated fungi, which were then compared to the literature (Crous and Gams 2000; Yan et al. 2013; Silva et al. 2017; Yang et al. 2017). Occurrences of *Botryosphaeria* spp. (black dead arm), *Phaeoconiella chlamydospore*, and *Phaeoacremonium* spp. (Petri disease and Esca disease complex) were identified.

For the virus diagnosis, extractions from 1 g of petioles, leaf veins, or scrapings of mature stems were performed for the viral identification of the total RNA, using the adsorption of nucleic acids on silica particles (Rott and Jelkmann 2001). Grapevine plants exhibiting typical leafroll symptoms were analyzed for six leafroll-related species (*Grapevine leafroll-associated virus*, GLRaV-1, -2, -3, -4, -5, and -7) by real-time RT-PCR (RT-qPCR). In all performed analyses, RNase-free water, healthy grapevines, and positive controls were included. Real-time RT-PCR reactions (One Step RT-PCR) were carried out in 96-well plates using the kit TaqMan Fast Virus 1-Step Master Mix (Life Technologies) and the thermocycler StepOnePlus Real-time PCR System (Applied Biosystems) (Dubiel et al. 2013). The primers and fluorescent probes used for viruses detections by RT-qPCR have been previously described (Osman et al. 2007). The shape of the curves and the quantification cycle obtained during the amplifications were as expected for virus amplification, and only GLRaV-3 was detected in the tested samples.

### Sampling procedures

To best capture the GLRaV foliar symptoms, which are apparent during the late summer and early fall (Mac Donald et al. 2016), leaves were collected in May 2015, 2016, and 2017, corresponding to the end of 2014/2015, 2015/2016, and 2016/2017 vegetative seasons.

Asymptomatic leaves were green colored, exhibited no discoloration or disease symptoms and morphological characteristics (color, shape, size) according to the cultivar ampelography (Galet 2002) (Fig. 1a). Leaves were collected from the diagnosed plants with the following symptoms, edge-down curl, red-violet leaf limb, and green-colored main veins for GLRaV (Fig. 1b); discrete leaf yellowing and beginning of rib discoloration for initial GTDs (Fig. 1c), chlorosis or interventional necrosis and reddish/purple discoloration surrounded by yellowish discoloration, standard symptom of “brindle stripes” for final GTD (Fig. 1d). At the end of the

grapevine cycle (May), it was possible to find leaves with consolidated GLRaV symptoms and, in case of GTDs, leaves with consolidated (final) and initial symptoms, so, to represent the real situation observed in the vineyards, GTDs leaves in both situations (initial and final) were sampled.

Every May (2015, 2016, and 2017), fresh leaves were collected (between 9 p.m. and 11 p.m.), grouped by treatment in paper bags and kept refrigerated (between 6 and 10 °C) until being transported to the lab. The objective was to maintain leaf tissue characteristics by preventing freezing or excessive water loss. The leaves were transported to the lab in the paper bags stored in a styrofoam box. At the end of the three vegetative seasons, in a total of 80 leaves (20 leaves per treatment) had been submitted to hyperspectral measurements.

### Spectral measurements

Leaf reflectance was measured using the non-imaging high-resolution spectroradiometer FieldSpec 3 (Analytical Spectral Devices – ASD, Panalytical Company, Boulder, CO, USA) with 350 to 2500 nm spectral range and 3 nm spectral resolution (Full-Width-Half-Maximum - FWHM) at 700 nm, 10 nm FWHM at 1400 nm, and 10 nm FWHM at 2100 nm (ASD 2010). This spectroradiometer operates with three separate detectors (VNIR: 350 to 1000 nm spectral region; SWIR 1: 1000 to 1830 nm; SWIR 2: 1830 to 2500 nm) and each detector is covered by order separation filters to eliminate second and higher-order effects (ASD 2010).

Following data acquisition (leaf), the original data was internally processed and integrated with the calibration measurement previously performed with Spectralon reference plate (white reference standard) to have a spectrum that expressed the reflectance over the whole spectral domain continuously and free of significant jumps between the spectral domains of each sensor. All spectral measurements were collected from the leaf adaxial surface using a leaf clip assembly attached to a plant probe. For all treatments, the measurements were made in the same way: the clip was positioned on two portions of the leaf with characterized symptoms (symptomatic leaves) or two portions without symptoms (asymptomatic leaves). For each leaf portion, three spectra were obtained (six measurements per leaf;  $n = 480$ ). The spectral profile of each leaf was calculated using the average of the six measurements per leaf and normalized by the maximum in the Chemostat software (Helfer et al. 2015).

### Data processing

To investigate the possibility of grouping, leaf spectrum data (average and normalized by the maximum) were transformed by the first derivative and, after excluding the atypical data (by the Hotelling  $T^2$  method;  $p < 0.05$ ), submitted to principal component analysis (PCA) (centered on the mean). PCA is a

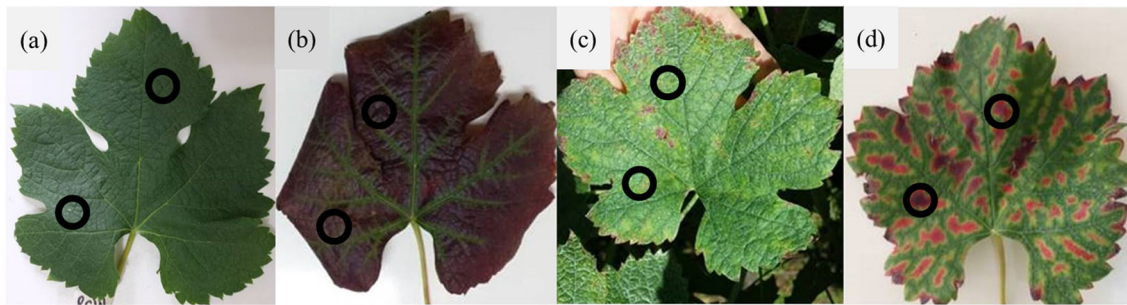


**Fig. 1** Examples of grapevine (*V. vinifera* cv. Merlot) leaves without (a) and with (b, c, d) symptoms of diseases associated to plant decline in vineyards: (a) asymptomatic leaves exhibited green colored, no discoloration, and disease symptoms; (b) symptomatic leaves to grapevine leafroll-associated virus (GLRaV) exhibited edge-down curl, red-violet leaf limb, and green-colored main veins; symptomatic leaves to grapevine trunk diseases (GTDs) exhibited discreet leaf yellowing and

beginning of rib discoloration for initial GTDs (c); chlorosis or interventional necrosis and reddish/purple discoloration surrounded by yellowish discoloration, standard symptom of “brindle stripes” for final GTD (d). Open black circles indicate the leaf clip positions during the hyperspectral measurements with spectroradiometer (spectral range 350 to 2500 nm)

multivariate statistical analysis exploratory method that was used to analyze the possibility of spectral separation between leaves with and without the GTDs and GLRaV symptoms. PCA score graphic shows the grouping tendency and the PCA loadings show the main wavelengths associated with the PCA score. PCA was performed by the Chemostat software (Helfer et al. 2015). Hotelling  $T^2$  is one of the methods for measuring the variation within the PCA model to identify possible outliers, based on the generalization of Student’s  $t$  statistic for the multivariate case, according to the sample estimates of the covariance matrices (Helfer et al. 2015).

The spectral separation of classes was performed using the partial least squares discriminant analysis (PLS-DA), with component 1 and component 2 defined by PCA. In our study, PLS-DA was performed as a descriptive model using the R software (Core Team 2018) package “mixOmics” (Rohart et al. 2017). PLS-DA is an algorithm used for predictive and descriptive modeling as well as for discriminative variable selection (Lee et al. 2018). PLS-DA is an extension of the classical PLS regression algorithm that allows robust model fitting when the model is overspecified (more predictors than observations) (Couture et al. 2018).

Differences between classes were subsequently analyzed using the average spectrum per class ( $n = 15$  to 20), difference-spectrum, and first-order derivative (FOD) spectra. The difference spectrum was determined by subtracting the average spectrum of asymptomatic leaves from the GTDs (initial and final) and GLRaV average spectrum. The difference spectrum shows differences (expressed as normalized reflectance values) between symptomatic and asymptomatic leaves (consider, in this case, the “zero line”) in every wavelength. FOD transformation of the spectral curve is a common technique applied to increase discrimination quality by enhancing spectral features and minimizing random noise (Demetriades-Shah et al. 1990).

Variable importance in the projection (VIP) analysis was performed to select the relevant wavelengths for class

separation. Wavelength selection techniques reduce the predictor space and provide a reduced set of wavelengths that can be used as efficiently to predict the response variable (Heim et al. 2018). The VIP analysis was performed from the normalized dataset using the PLS-VIP method. Chong and Jun (2005) reported that the PLS-VIP method excelled when identifying relevant predictors and outperformed other methods. For the wavelength selection, the VIP values  $> 1.0$  in components 1 and 2 were considered to identify unique features for each class (VIP values  $> 1.0$  and no overlap) using the software R (Core Team 2018) package “vip” (Greenwell et al. 2018). Since the average of squared VIP scores equals 1, “greater than one rule” is generally used as a criterion for variable selection (Chong and Jun 2005).

## Results

In the PCA analysis, PC1 and PC2 explained 60.5% of the spectral variance, forming four groups in the PC1 (39.55%) versus PC2 (20.99%) projection (Fig. 2a). Asymptomatic leaves and final GTD symptomatic leaves were positioned in the PC1 with an opposite projection: positive to the first ones and negative to the latter. PC2 assigned positive scores to leaves with GLRaV symptoms and negative scores to leaves with initial GTD symptoms (Fig. 2a). The variables used for grouping the samples are observed in the principal component loading graphs (Fig. 2b, c). In PC1, the variables with the highest contribution were wavelengths between 700 and 740 nm, centered at 720 nm (Fig. 2b), whose positive weight can be strongly associated with asymptomatic leaves whereas the wavelength 690 nm (negative weight) may be associated with leaves with final GTD symptoms. In PC1, the contribution of wavelengths between 560 and 630 nm may also be associated with leaves displaying both initial GTD and GLRaV symptoms since both samples are in the negative portion of PC1. In PC2, there was a greater contribution of

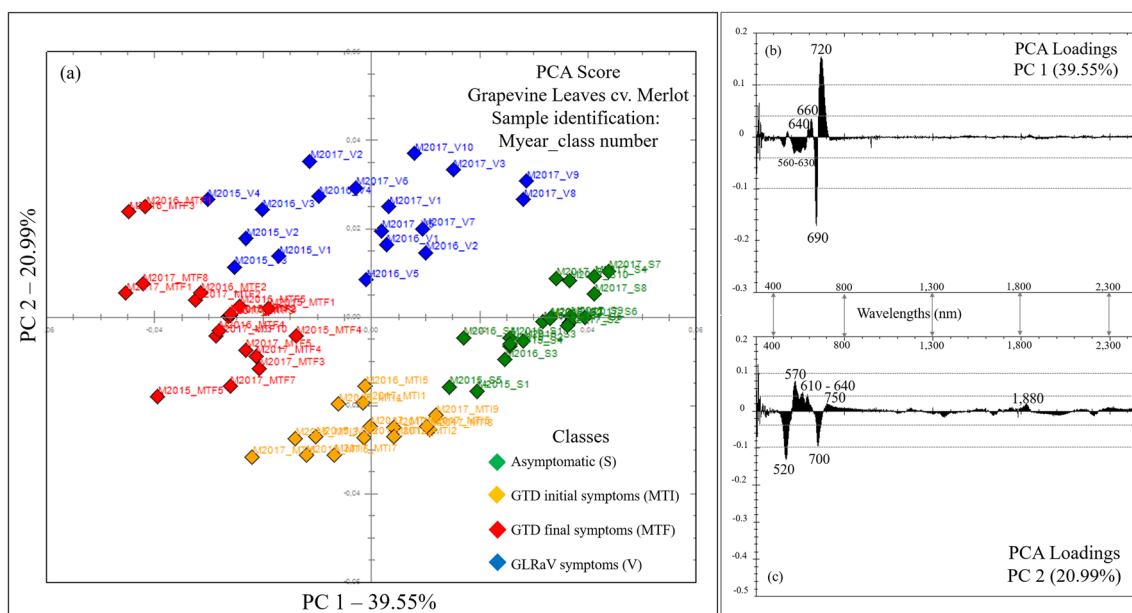


**Fig. 2** Principal components analysis (PCA) score (a) showing the tendency of spectral separation of the grapevines (*V. vinifera* cv. Merlot) leaves in classes: asymptomatic (S, symbols in green) and symptomatic to grapevine leafroll-associated virus (GLRaV) (V, symbols in blue) and to grapevine trunk diseases (GTDs) with initial

(MTI, symbols in orange) and final (MTF, symbols in red) symptoms; (b) Principal component 1 (PC1) and principal component 2 (PC2) loadings for hyperspectral reflectance (350–2500 nm) of asymptomatic (S) and symptomatic (V, MTI and MTF) grapevine leaves with the main wavelengths associated with the PCA score (a) in highlight

wavelength 570 nm (Fig. 2c), whose positivity is strongly associated with leaves with GLRaV symptoms. Negative weights of 520 and 700 wavelengths were strongly associated with the initial GTD, although the contribution of asymptomatic and final GTD leaves cannot be excluded.

Like the first non-supervised analysis, PCA results showed a tendency to the spectral separation of the grapevines leaves in classes. Zhang et al. (2002), through PCA, observed a high positive linear correlation of the first component with the canopy spectra of healthy tomato plants and the second component with the *Phytophthora infestans* infected plants. Likewise, our PCA score indicated that the percentage of samples in negative PC1 increased with the advancing GTD symptoms (initial to final) and most GTD and all GLRaV samples were PC2 positive (Fig. 2a), showing that this component (PC2) can be associated with symptomatic leaves.

In this study, the two main components defined by the PCA (Fig. 2a) were used to adjust the PLS-DA. The results of the PLS-DA score indicated the separation in groups, confirming the existence of a spectral distinction between asymptomatic and GTD and GLRaV symptomatic leaves (Fig. 3). The PLS-DA scores formed four separate groups in the dispersion space that were associated with the previously identified classes (Fig. 3). Leaves with GLRaV symptoms were considered spectrally distinct from the others due to X positive score while the final GTD is spectrally distinguished from the asymptomatic and GLRaV classes by the positive score in Y and negative in X. Two classes were positioned in the negative X and negative Y quadrants, the asymptomatic and initial

GTD (Fig. 3). This result was considered coherent because leaves with GTD initial symptoms exhibit portions of green-colored leaf area (Fig. 1c); therefore, comparatively, these leaves are more similar to asymptomatic leaves.

The average normalized spectra also indicated differences between grapevine leaf classes (Fig. 4a). The average normalized spectra of asymptomatic leaves had the typical spectral

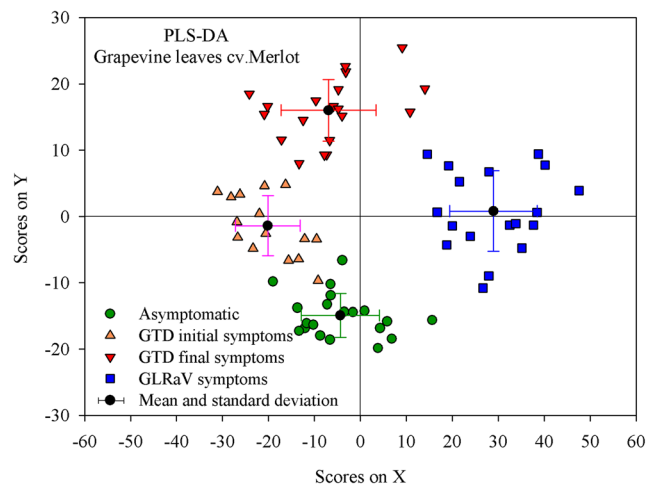


**Fig. 3** Ordination plot of the mean and standard deviation of first two spectral axes (X and Y) resulting from partial least squares discriminant analysis (PLS-DA) showing the hyperspectral dissimilarity between grapevine leaves (*V. vinifera* cv. Merlot) asymptomatic (symbols in green) and symptomatic to grapevine leafroll-associated virus (GLRaV, symbols in blue) and grapevine trunk diseases (GTDs) with initial (GTD initial, symbols in orange) and final (GTD final, symbols in red) symptoms

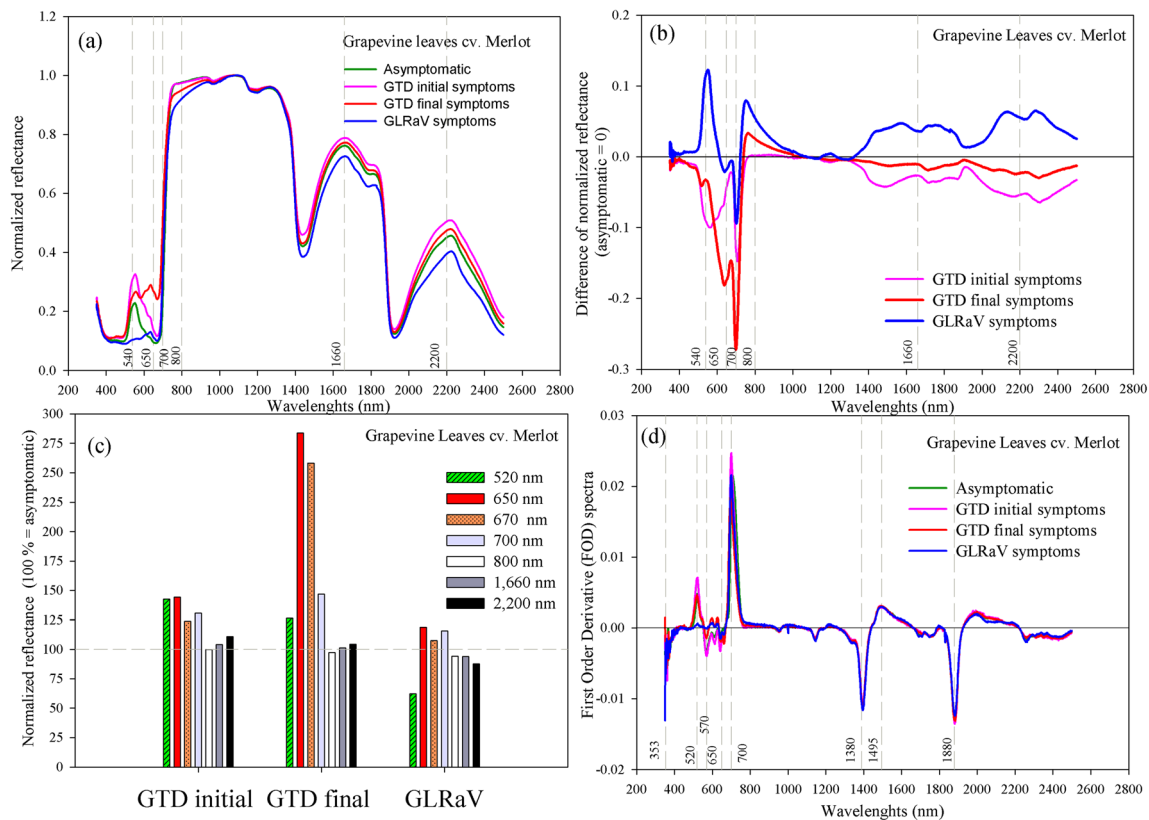


**Fig. 4** Hyperspectral behavior (350–2500 nm) of grapevine leaves (*V. vinifera* cv. Merlot), asymptomatic, symptomatic to grapevine leafroll-associated virus (GLRaV), and symptomatic to grapevine trunk diseases (GTD) with initial symptoms (GTD initial) and final symptoms (GTD final) expressed in terms of (a) normalized reflectance; (b) normalized difference reflectance that indicated the differences between symptomatic and asymptomatic leaves (consider, in this case, the “zero line”); (c) percentage of reflectance of symptomatic leaves (GLRaV, GTD initial, and GTD final) considering asymptomatic equal 100% in

important wavelengths associated to spectral behavior of vegetation in visible (VIS) range (green edge 520 nm, chlorophyll *b* 650 nm, chlorophyll *a* 670 nm, red edge 700 nm), near-infrared (NIR) range (represented, in this case, by 800 nm), and shortwave infrared (SWIR) range (represented, in this case, by 1660 nm and 2200 nm) and (d) first-order derivative (FOD) that enhancing spectral features of the hyperspectral behavior of asymptomatic and GLRaV, GTD initial, and GTD final symptomatic grapevine leaves

behavior of photosynthetically active green vegetation with absorption bands of electromagnetic radiation by chlorophylls in blue (450 nm) and red (650–670 nm), green reflectance peak (520–540 nm), and higher reflectance values compared to visible light in the near-infrared (Fig. 4a). The reflectance values were different in leaves with disease symptoms related to vine decline compared to asymptomatic leaves (Fig. 4a, b), showing that the structural and physiological changes promoted by the pathogens modified the interaction between the electromagnetic radiation and the leaf tissue.

In the visible range, at the green edge (520–550 nm), the normalized average spectra (Fig. 4a) and the difference spectra (Fig. 4b) indicated that the reflectance increased, varying between 26.5% (final symptoms) and 43% (initial symptoms) (Fig. 4c), in leaves with GTD symptoms compared to asymptomatic ones. On the other hand, leaves with GLRaV symptoms had very low reflectance values in the visible light wavelengths, including the green edge (Fig. 3a), equivalent to 62% of asymptomatic reflectance (Fig. 4d).

The results also show that leaf reflectance behaved differently in the red range. In the presence of GTD symptoms, leaf reflectance increased in the 650 nm wavelength (Fig. 4a, b, and c), especially in those with advanced symptoms due to markedly reduced absorption by chlorophyll *b* (650 nm). In this wavelength, leaf reflectance was 44% and 184% higher in the GTD initial and final stages compared to the asymptomatic leaves (Fig. 4c). At 670 nm (wavelength associated with chlorophyll *a*), leaf reflectance increased 24% and 158% for initial and final GTD symptoms, respectively (Fig. 4c). Furthermore, reflectance also increased in GLRaV leaves at wavelengths 650 nm (18% increase) and 670 nm (8% increased) albeit to a lesser extent compared to those with GTD symptoms (Fig. 4c). Reflectance increases near 700 nm wavelengths were evidenced in all symptomatic leaves (Fig. 4b, c).

Asymptomatic leaves had spectral behavior typical of green vegetation in the near-infrared (NIR, 700 to 1300 nm) (Fig. 4a). The spectral behavior of leaves with final GTD and GLRaV symptoms changed the most at the beginning of near-

infrared (700 to 900 nm) (Fig. 4b). Lower reflectance values were observed for GLRaV and final GTD in leaves characterized by consolidated disease symptoms. At 800 nm, reflectances were 2.6% and 5.6% lower in leaves with final GTD and GLRaV symptoms, respectively, compared to asymptomatic leaves (Fig. 4c).

In the shortwave infrared (SWIR, 1300 to 2500 nm), reflectance values increased in leaves with GTD symptoms, especially initial GTD, while reducing for the GLRaV symptoms (Fig. 4a). At 1660 nm and 2200 nm, wavelengths associated with plant phenolic absorption (Kokaly and Skidmore 2015), the reflectance was 4% higher in leaves with initial GTD symptoms compared to asymptomatic leaves, and 6.2% lower in GLRaV leaves.

In remote sensing, the first-order derivative of reflectance spectra is used to locate the wavelength of maximum slope of the reflectance in the red-edge spectral region (RESR) (680–730 nm). In this study, the FOD spectrum peaks were observed at 705 nm (asymptomatic leaves), 700 nm (initial GTD and GLRaV), and 698 nm (final GTD) (Fig. 4d), indicating a spectral blueshift of the red edge. The FOD spectrum peaked also at 520 nm for asymptomatic and GTDs symptomatic leaves; however, no peak was detected to GRLaV symptomatic leaves (Fig. 4). The FOD spectra of asymptomatic, GTD, and GLRaV symptomatic leaves also indicated one positive (~1500 nm) and three negative (1400 nm, 1900 nm, and 2500 nm) peaks. The negative peaks are associated with the strong water absorption bands found in the SWIR region, centered on 1450, 1940, and 2500 nm.

The VIP results indicated the important wavelengths for identifying and projecting characteristic reflectance values for asymptomatic as well as GTD and GLRaV symptomatic leaves (Fig. 5). Asymptomatic and symptomatic leaves could be discriminated in component 1 as a function of VIPs > 1 at the 520–600 nm, 1000–1060 nm ranges, and SWIR region (Fig. 5a, b, c), allowing to assign these bands as spectral markers of leaves without the evaluated diseases' symptoms. The 640–660 nm range has been identified in the PCA loading (Fig. 2b) and, finally, confirmed as an important VIP in component 2 (Fig. 5d, e, f) for identifying changes in the spectral signature of grapevine decline-related diseases, although it does not differentiate between diseases.

The VIP analysis component 2 discriminated between diseases by wavelength ranges: initial GTD presented VIPs > 1 for wavelengths greater than 1140 nm (up to 2400 nm) so that the SWIR could be considered an important spectral feature for initial GTD symptoms (Fig. 5d). The VIP peak in the 950–1000 nm region (Fig. 5e) identifies this range as a spectral marker for GTD final symptoms, as well as at 1900 nm peak (Fig. 5e). Wavelengths in the 500–520 nm range appear as VIP to GLRaV, as did the peaks at 1400 nm and 1880 nm (Fig. 5f). Previously identified as important by the PCA loading (Fig. 2c) and confirmed by the VIP analysis, the green

peak indicated the 500–520 range could be an important marker to discriminate GRLaV symptomatic leaves (Fig. 5f).

## Discussion

In this study, we showed that spectral response of asymptomatic grapevine leaves can be distinguished from symptomatic to two important diseases associated with vineyard decline. The successful leaves discrimination is based on the characteristic effect of the pathogens, being also possible to establish a link between the hyperspectral information and the biochemistry and physiology changes described in the literature for GTD and GLRaV, highlighting the disease physiology like the origin of the capacity to use spectroscopy for plant-pathogen interaction understanding.

The reflectance increase observed in leaves with GTD symptoms at the green edge was especially associated with the reduced total chlorophyll and, to a lesser extent, with carotenoids, since the carotenoid content is reportedly stable during a GTD infection (Petit et al. 2006; Magnin-Robert et al. 2011). Additionally, Gitelson and Merzlyak (1996) showed that traces of chlorophylls *a* and *b* and significant content of carotenoids did not change leaf reflectance at 540 nm, suggesting a lesser spectral contribution of carotenoids compared to chlorophylls. The increase in VIS reflectance noted in GTD symptomatic leaves was also reported in other studies that described the hyperspectral behavior of leaves with fungal disease symptoms, like in downy mildew symptomatic grapevine leaves (Calcante et al. 2012; Oerke et al. 2016), sugar beet leaves with symptoms of *Cercospora* leaf spot, powdery mildew and sugar beet rust (Mahlein et al. 2010), and olive leaves obtained from *Xylella fastidiosa* infected trees (Poblete et al. 2020).

Leaves with GLRaV symptoms had very low reflectance values in the visible light wavelengths; thus, the spectral behavior indicates very little pigment absorption, agreeing with Gutha et al. (2010) and Basso et al. (2017) that also reported fewer total chlorophylls and carotenoids in GLRaV leaves compared to healthy green leaves. Likewise, Naidu et al. (2009) also indicated near 540 nm wavelengths as important for GLRaV-3 spectral discrimination in “Cabernet Sauvignon” leaves. The lack of reflectance at 520 nm highlights the antagonistic behavior among classes in this wavelength and may be due to the purplish coloration associated with anthocyanin accumulation in GLRaV symptomatic leaves. Gutha et al. (2010), using a spectrophotometer, did not detect anthocyanins in virus-free green leaves whereas anthocyanins and increased flavanols were apparent in virus-infected leaves.

The reflectance increase observed at wavelengths related to photosynthetic pigments (650 and 670 nm) was associated with the reduced chlorophyll index in GTD leaves (Junges

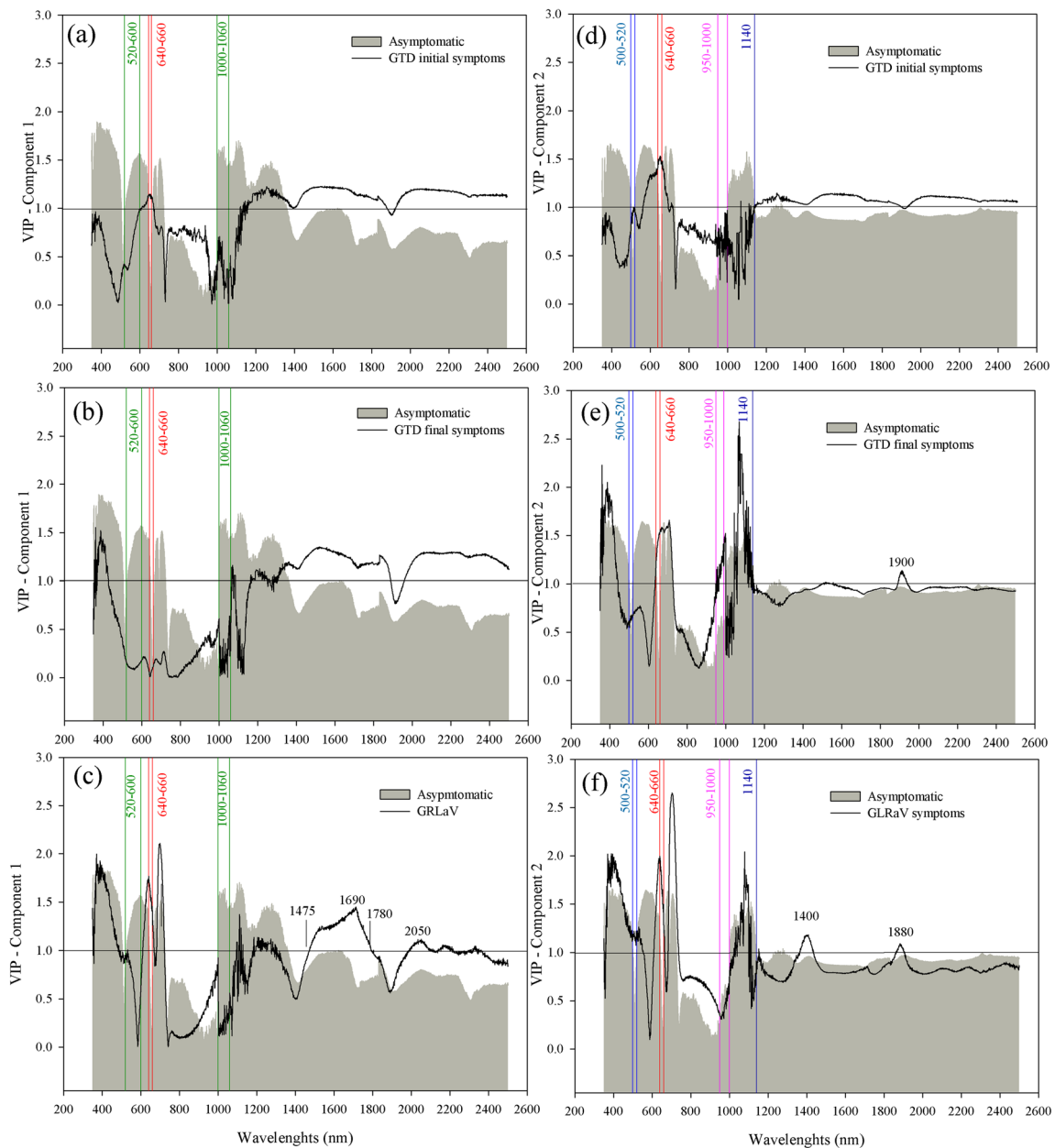


**Fig. 5** Scores of variable importance in the projection (VIP) in component 1 (a, b, c) and component 2 (d, e, f) to grapevine leaves (*V. vinifera* cv. Merlot) asymptomatic (gray area) and symptomatic to grapevine leafroll-associated virus (GLRaV) and grapevine trunk diseases (GTDs) with initial symptoms (GTD initial) and final

symptoms (GTD final) (black lines). Values >1.0 indicate the most important wavelengths to class separation. Wavelengths with VIP values >1.0 in components 1 and 2 and no overlap were highlighted to identify unique features to each class

et al. 2018) and the strong drop of both yields, the maximum fluorescence, and effective Photosystem II quantum, due to GTD pathogens (Petit et al. 2006; Magnin-Robert et al. 2011). Vanegas et al. (2018) also reported that “Chardonnay” vines infested with phylloxera (*Daktulosphaira vitifoliae*) have higher reflectance levels in the wavelengths associated with chlorophyll while the 680 nm wavelength highlights the main differences between uninfested and infested spectral signatures. Delalieux et al. (2007) demonstrated that apple trees with biotic stress (*Venturia inaequalis*) impacted the most

the reflectance values in the 580–660 nm range, corresponding to the chlorophyll absorption regions. Mahlein et al. (2010) reported an increase in VIS mostly in green and red ranges (500–700 nm) in sugar beet leaves infected with *Cercospora beticola* leaf spot and powdery mildew whereas a lesser increase was detected in leaves with sugar beet rust, probably due to the mild symptoms observed in the leaf area. For viruses, Naidu et al. (2009) also defined that the two maximum differences in the visible region occur at the green (540 nm) and red (680 nm) peaks indicating less

chlorophyll absorption by the GLRaV-3 infected leaves. Gutha et al. (2010) indicated that total chlorophylls and carotenoids were, respectively, 20.1% and 19.8% less in GLRaV-3 symptomatic leaves compared to green ones.

Sensitivity to chlorophyll concentrations and to metabolic disturbances can be identified near the 700 nm wavelengths, range that belongs to the red edge, a unique feature of green vegetation resulting from two optical properties of asymptomatic leaves, the high absorption of chlorophyll *a* in the 670 nm and the high reflectance due to the internal leaf scattering in longer wavelengths (near-infrared) (Gitelson and Merzlyak 1996). Likewise, Carter and Knapp (2001) showed in earlier studies that, frequently, the steep slope of reflectance curves in the far-red spectrum can produce the illusion that stress-induced differences are negligible near 700 nm. However, the simple subtraction of control curves (asymptomatic leaves) from curves representing the stressed condition (symptomatic leaves) shows clearly the far-red response.

Hyperspectral studies have used derivatives to define the wavelength position of the red edge and illustrate the relationships between the red edge and total chlorophyll concentration in leaves. FOD indicated a spectral blueshift of the red edge in the grapevine leaves analyzed in this study. Because leaf reflectance red edge was highly correlated with chlorophyll, the shift of the red edge towards the blue wavelengths is associated with lower chlorophyll content (Demetriades-Shah et al. 1990). Therefore, the difference between asymptomatic and GTD and GLRaV symptomatic red edge position was likely associated with the reduction in chlorophyll due to the presence of pathogens. However, the blue shift to the red edge indicates the occurrence of plant stress, being not a specific disease spectral marker. In this study, FOD spectra also indicated a negative peak in 353 nm especially in GLRaV symptomatic leaves, a wavelength associated with flavonols (Gutha et al. 2010); however, this result needs to be viewed with caution because wavelengths below 400 nm have more spectral noise and this part of the spectra tends to be removed in some studies (Heim et al. 2018; Gold et al. 2019; Mahlein et al. 2010).

In the NIR range, the spectral behavior of green vegetation is characterized by high reflectance values compared to visible light so that higher reflectance values were expected in asymptomatic leaves resulting from non-absorption of radiation to avoid heating and damage to the plant tissue (Jensen 2007). Leaves with well-defined symptoms (final GTD and GLRaV) displayed decreased reflectance in NIR and no near-infrared changes for initial GTD. This NIR decrease has been reported in several studies on changes in leaf spectral signatures associated with occurring pathogens (Mahlein et al. 2010; Calcante et al. 2012; Knauer et al. 2017; Heim et al. 2018; Couture et al. 2018). Even if smaller than those observed in visible light, the depressions at near-infrared reflectance are indicators of changing or general loss of functionality of leaf

tissue. Chlorosis and necrosis of leaf tissues are the main symptoms of final GTD so the obvious hypothesis is that leaf chlorophyll content decreases (therefore, changing the photosynthetic process) while cells die as well. In fact, it has been shown that leaf stripe symptoms (GTD) are preceded and/or accompanied and even followed by morphological and physiological modifications of both leaf tissue and photosynthetic apparatus (Masi et al. 2018). Valtaud et al. (2009) reported that the intracellular structures of symptomatic GTD leaves were damaged more extensively in the chlorotic parts, as the tonoplasts were disrupted. Like other trunk disease pathogens, *Phaeoacremonium* spp. and *P. chlamydospora* produce toxic metabolites as scytalone, isosclerone, flaviolone, hydroxybenzoic acid, some exopolysaccharides, and the most common action mode of these metabolites are related to their oxidant property (Andolfi et al. 2009).

Spectral signatures of symptomatic GTD and GLRaV leaves compared with asymptomatic differed in the SWIR range, while SWIR reflectance increased in GTD symptomatic leaves, the spectral signature of GLRaV symptomatic leaves decreased. Reflectance increments in shortwave infrared are likely associated with a lower water content in the leaf as the SWIR reflectance is influenced by the leaf chemical composition and water (Carter and Knapp 2001). Masi et al. (2018) reported that GTD symptomatic leaves exhibited closure of stomata, damage to cellular organelles, decrease in starch grains, and a strong decrease of the stomatal conductance values. The GTD-affected plants suffer from slight water stress and modified concentration of the chemical markers, which increased over time as if there was a progressive accumulation of toxic substances in the leaves (Masi et al. 2018). Botryosphaeriaceous species (*Botryosphaeria* spp.) can produce toxic metabolites from different compound classes including aromatic compounds, isocoumarins, jasmonates, naphthalenones, polyketides, and phenols (Martos et al. 2008; Masi et al. 2018; Reveglia et al. 2019). Heim et al. (2018) also reported increased SWIR reflectance in the hyperspectral signature of untreated lemon myrtle trees compared to fungicide-treated to eliminate myrtle rust while linking the SWIR reflectance changes to changing leaf water content due to the water loss from lesions observed in untreated leaves. Knauer et al. (2017) also reported a shift between the mean spectral signatures of healthy detached berries and those with severe powdery mildew infection due to higher reflectance of the diseased berries throughout the SWIR region. Our results showed decreased SWIR reflectance in GLRaV symptomatic leaves. Thus, leaves with GLRaV symptoms appear to have higher water content and, since water is a good energy absorber, the higher the turgidity of plant tissue, the lower the reflectance values in SWIR. In this spectral range, the green vegetation reflectance peaks occur mainly at 1600 nm and 2200 nm, the wavelengths between two atmospheric water main absorption bands (1440 nm and

1940 nm) whereas leaves with GLRaV symptoms had lower reflectance values in 1600 and 2200 nm, compared to asymptomatic ones. Naidu et al. (2009) also identified reflectance reduction at wavelengths close to 1600 and 2200 nm, which may be associated with sugar and starch accumulation in leaves with GLRaV symptoms. Cell-to-cell viral movement occurs through plasmodesmata, mediated by the viral movement protein. This fact coupled with virus replication and concentration preferentially in phloem tissues could disorganize these tissues, with negative effects on photoassimilate translocation, leading to starch accumulation in GLRaV leaves (Basso et al. 2017).

Moreover, the wavelengths 1660 nm and 2200 nm are associated with phenolic compounds that can be accumulated in the cell in response to pathogens. Kokaly and Skidmore (2015) observed that the narrow features at 1660 nm and 2140 nm were consistent with absorption caused by aromatic C-H bond in the chemical structure of phenolic compounds and non-hydroxylated aromatics. A study by Gold et al. (2020) showed wavelengths around 2100 nm allowed to discriminate potato leaves symptomatic to late blight (*Phytophthora infestans*) and early blight (*Alternaria solani*), highlighting that differences in phenolic concentration are important to detect and differentiate disease. The lower reflectance of GLRaV symptomatic leaves at 1660 nm and 2200 nm could be associated with the presence of anthocyanins, a phenolic compound belonging to the flavonol group. Gutha et al. (2010) found 24% higher levels of flavonols in virus-infected symptomatic leaves than in virus-free green leaves, with quercetin followed by myricetin as the predominant compounds. The flavonoid biosynthetic pathway occurred in GLRaV-3-infected leaves of a red-fruited wine grape cultivar (cv. Merlot) leading to *de novo* synthesis of two classes of anthocyanins. These anthocyanins have contributed to the expression of the reddish-purple color of virus-infected grapevine leaves exhibiting GLRD symptoms (Gutha et al. 2010).

The spectral signatures of symptomatic GTD and GLRaV leaves in SWIR and the selection of some VIP wavelengths in this range indicated that the pathogen probably induced important biochemical, physiological, and morphological changes in the leaf tissue that allow discriminating symptomatic from asymptomatic leaves. However, due to the several narrow bands of absorption located in SWIR associated to protein, cellulose, lignin, and starch (Curran 1989), more studies and, probably, physiological testing are necessary to establish the relationship between the compounds specific to plant-pathogen interaction and the spectral reflectance before a strong conclusion.

The successful discrimination between spectral signatures of asymptomatic and GTD and GLRaV symptomatic leaves is the first step towards using spectral approaches to detect and monitor diseases associated with the decline and plant death in

vineyards. Our results defined that the spectral signatures of symptomatic leaves are different from the asymptomatic while being always possible to link the reflectance changes in VIS, NIR, and SWIR to the plant-pathogen interactions described for a deeper understanding of optical properties during pathogenesis. VIP analyses reduced the high dimensionality of the hyperspectral data by eliminating irrelevant or redundant wavelengths or spectral ranges, defining spectral patterns that can be employed for identifying and monitoring disease in vineyards. Some wavelength ranges appointed in this study were also cited as VIP by other authors and could be considered important to discriminate between healthy and diseased leaves (Heim et al. 2018; Knauer et al. 2017; Gold et al. 2019, 2020). The 500–520 nm and wavelengths near 1660 nm (as VIP 1690 nm) for GLRaV symptomatic leaves and the 950–1000 nm range for final GTDs could be highlighted. Here, a first set of the most important wavelengths to discriminate asymptomatic and GTD's and GLRaV symptomatic grapevine leaves was identified to provide future studies a starting point for validation or further classification tests and, likewise, a disease-specific vegetation index could be developed by refining this first set of wavelengths. According to Mahlein (2016), regardless of all the positive and future benefits of using sensors for plant disease detection and monitoring, it must be taken into consideration that interpreting the sensor data is crucial. Depending on the goals, just a few regions of the spectral range may be of interest. Using a relatively small number of wavelengths, the detection equipment can be tailored to suit a specific plant-pathogen interaction, reducing the cost of the final sensor (Mahlein 2016).

Establishing spectral signatures and the feasibility of spectral discrimination between asymptomatic and symptomatic GTD and GLRaV grapevine leaves have not been previously investigated. The results suggest that the spectral approach could be useful to promote the quantitative and qualitative analysis of the spatiotemporal distribution of affected plants, in the context of precision viticulture, or to regional disease monitoring and mapping by remote sensors. This conclusion is very important to the Serra Gaúcha region since there are no estimates on the vineyard areas affected by diseases related to grapevine decline and death. Further studies should be conducted on the potential use of hyperspectral reflectance for diagnosing grapevine decline diseases considering the phenological cycle, disease severity stages, and differences between cultivars in terms of response to pathogens, especially because unlike red-wine cultivars (like “Merlot”), the white-wine cultivars do not have the phenotypic expression of reddish-purple coloration of leaves with GLRaV symptoms.

**Authors' contributions** Conceptualization: [Amanda Heemann Junges]; Data curation: [Amanda Heemann Junges] and [Jorge Ricardo Ducati]; Methodology: [Amanda Heemann Junges], [Jorge Ricardo Ducati], [Marcus André Kurtz Almança] and [Thor Vinicius Martins Fajardo];

Formal analysis and Project administration: [Amanda Heemann Junges]; Writing—original draft preparation: [Amanda Heemann Junges], [Marcus André Kurtz Almança] and [Thor Vinicius Martins Fajardo].

**Funding information** This study was supported by the Marin family, owner of the studied vineyard, the Brazilian National Council for Scientific and Technological Development (CNPq, process 473398/2013-3), Federal Institute of Rio Grande do Sul/Campus Bento Gonçalves (IFRS/BG), and Rio Grande do Sul State Research Foundation (FAPERGS).

## References

- Almança MAK, Abreu CM, Scopel FB, Benedetti M, Halleen F, Cavalcanti FR (2013) Evidências morfológicas da ocorrência de *Phaeoconiella chlamydospora* em videiras no Estado do Rio Grande do Sul. Comunicado Técnico-Embrapa Uva e Vinho 134: 1–5
- Alvares CA, Stape JL, Sentelhas PC, Gonçalves JLM, Sparovek G (2013) Köppen's climate classification map for Brazil. Meteorologische Zeitschrift 22:711–728
- Andolfi A, Cimmino A, Evidente A, Iannaccone M, Capparelli R, Mugnai L, Surico G (2009) A new flow cytometry technique to identify *Phaeoconiella chlamydospora* exopolysaccharides and study mechanisms of esca grapevine foliar symptoms. Plant Disease 93:680–684
- ASD (2010) FieldSpec@3 user manual. Ed. Analytical Spectral Devices, Boulder
- Basso MF, Fajardo TVM, Hotelling P (2017) Grapevine virus diseases: economic impact and current advances in viral prospection and management. Revista Brasileira de Fruticultura 39:e-411
- Calcante A, Mena A, Mazzeto F (2012) Evaluation of 'ground sensing' optical sensors for diagnosis of *Plasmopara viticola* on vines. Spanish Journal of Agricultural Research 10:619–630
- Carter GS, Knapp AK (2001) Leaf optical properties in higher plants: linking spectral characteristics to stress and chlorophyll concentration. American Journal of Botany 88:677–684
- Chong IG, Jun CH (2005) Performance of some variable selection methods when multicollinearity is present. Chemometrics and Intelligent Laboratory Systems 78:103–112
- Core Team (2018) R: a language and environment for statistical computing. R Foundation for statistical computing, Vienna, Austria. URL <https://www.R-project.org/>
- Couture JJ, Singh A, Charkowski AO, Groves RL, Gray SM, Bethke PC, Townsend PA (2018) Integrating spectroscopy with potato disease management. Plant Disease 102:2233–2240
- Crous PW, Gams W (2000) *Phaeoconiella chlamydospora* gen. et comb. nov., a causal organism of Petri grapevine decline and esca. Phytopathologia Mediterranea 39:112–118
- Curran PJ (1989) Remote sensing of foliar chemistry. Remote Sensing of Environment 30:271–278
- Delalieux S, Aardt JV, Keulemans W, Schrevels E, Coppin P (2007) Detection of biotic stress (*Venturia inaequalis*) in apple trees using hyperspectral data: non-parametric statistical approaches and physiological implications. European Journal of Agronomy 27:130–143
- Demetriades-Shah T, Steven MD, Clark JA (1990) High-resolution derivative spectra in remote sensing. Remote Sensing of Environment 33:55–64
- Di Gennaro SF, Battiston E, Di Marco S, Facini O, Matese A, Nocentini M, Palliotti A, Mugnai L (2016) Unmanned aerial vehicle (UAV)-based remote sensing to monitor grapevine leaf stripe disease within a vineyard affected by Esca complex. Phytopathologia Mediterranea 55:262–275
- Dubiela CR, Fajardo TVM, Souto ER, Nickel O, Eiras M, Revers LF (2013) Simultaneous detection of Brazilian isolates of grapevine viruses by TaqMan real-time RT-PCR. Tropical Plant Pathology 38:158–165
- Fallon B, Yang A, Lapadat C, Armour I, Juzwik J, Montgomery R, Cavender-Bares J (2020) Spectral differentiation of oak wilt from foliar fungal disease and drought is correlated with physiological changes. Tree Physiology 40:377–390
- Galet P (2002) Grape varieties. Cassell Illustrated, London 159p
- Garrido LR, Sônego OR, Gomes VR (2004) Fungos associados com o declínio e morte de videiras no Estado do Rio Grande do Sul. Fitopatologia Brasileira 29:322–324
- Gitelson AA, Merzlyak MN (1996) Signature analysis of leaf reflectance spectra: algorithm development for remote sensing of chlorophyll. Journal of Plant Physiology 148:494–500
- Gold KM, Townsend PA, Herrmann I, Gevens AJ (2019) Investigating potato late blight physiological differences across potato cultivars with spectroscopy and machine learning. Plant Science 2019, in press:110316
- Gold KM, Townsend PA, Chlus A, Herrmann I, Couture JJ, Larson ER, Gevens AJ (2020) Hyperspectral measurements enable pre-symptomatic detection and differentiation of contrasting physiological effects of late blight and early blight in potato. Remote Sensing 12:286
- Gramaje D, Úrbez-Torres JR, Sosnowski MR (2018) Managing grapevine trunk diseases with respect to etiology and epidemiology: current strategies and future prospects. Plant Disease 102:12–39
- Greenwell B, Boehmke B, Gray B (2018) vip: Variable Importance Plots. R package version 0.1.2. Available at: <https://CRAN.R-project.org/package=vip>
- Gutha LR, Casassa LF, Harbertson JF, Naidu RA (2010) Modulation of flavonoid biosynthetic pathway genes and anthocyanins due to virus infection in grapevine leaves. BMC Plant Biology 10:187
- Heim RHJ, Wright IJ, Chang HC, Carnegie AJ, Pegg GS, Lancaster EK, Falster DS, Oldeland J (2018) Detecting myrtle rust (*Austropuccinia psidii*) on lemon myrtle trees using spectral signatures and machine learning. Plant Pathology 67:1114–1121
- Helfer G, Bock F, Marder L, Furtado J, Costa A, Ferrao M (2015) Chemostat: exploratory multivariate data analysis software. Química Nova 38:575–579
- IBRAVIN. Instituto Brasileiro do Vinho: Brasil vitivinícola. Available at: <http://www.ibravin.org.br>. Accessed on June 25, 2019
- Jensen JR (2007) Remote sensing of vegetation. In: Jensen JR (ed) Remote sensing of the environment: an earth resource perspective. Upper Saddle River, Pearson Prentice Hall, pp 357–410
- Junges AH (2018) Caracterização climática da temperatura do ar em Veranópolis. Agrometeoros 26:299–306
- Junges AH, Ducati JR, Scalvi LC, Almança MAK (2018) Detection of grapevine leaf stripe disease symptoms by hyperspectral sensor. Phytopathologia Mediterranea 57:399–406
- Junges AH, Bremm C, Fontana DC (2019) Rainfall climatology, variability, and trends in Veranópolis, Rio Grande do Sul, Brazil. Revista Brasileira de Engenharia Agrícola e Ambiental 23:160–166
- Knauer U, Matros A, Petrovic T, Zanker T, Scott ES, Seiffert U (2017) Improved classification accuracy of powdery mildew infection levels of wine grapes by spatial-spectral analysis of hyperspectral images. Plant Methods 13:47
- Kokaly RF, Skidmore AK (2015) Plant phenolics and absorption features in vegetation reflectance spectra near 1.66  $\mu\text{m}$ . International Journal of Applied Earth Observation and Geoinformation 43:55–83
- Lee CL, Liong CY, Jemain AA (2018) Partial least squares-discriminant analysis (PLS-DA) for classification of high-dimensional (HD) data: a review of contemporary practice strategies and knowledge gaps. Analyst 143:3526–3539
- Mac Donald SL, Staid M, Staid M, Cooper ML (2016) Remote hyperspectral imaging of grapevine leafroll-associated virus 3 in

- cabernet sauvignon vineyards. *Computers and Electronics in Agriculture* 130:109–117
- Magnin-Robert M, Letousey P, Spagnolo A, Rabenoelina F, Jacquens L, Mercier L, Clément C, Fontaine F (2011) Leaf strip of esca induces alteration of photosynthesis and defence reactions in presymptomatic leaves. *Functional Plant Biology* 38:856–866
- Mahlein AK (2016) Plant disease detection by imaging sensors—parallels and specific demands for precision agriculture and plant phenotyping. *Plant Disease* 100:241–251
- Mahlein AK, Steiner U, Dehne HW, Oerke EC (2010) Spectral signatures of sugar beet leaves for the detection and differentiation of diseases. *Precision Agriculture* 11:413–431
- Martinelli F, Scalenghe R, Davino S, Panno S, Scuderi G, Ruisi P, Villa P, Stroppiana D, Boschetti M, Goulart LR, Davis CE, Dandekar AM (2015) Advanced methods of plant disease detection: a review. *Agronomy for Sustainable Development* 35:1–25
- Martos S, Andolfi A, Luque J, Mugnai L, Surico G, Evidente A (2008) Production of phytotoxic metabolites by five species of Botryosphaeriaceae causing decline on grapevines, with special interest in the species *Neofusicoccum luteum* and *N. parvum*. *European Journal of Plant Pathology* 121:451–461
- Masi M, Cimmino A, Reveglia P, Mugnai L, Surico G, Evidente A (2018) Advances on fungal phytotoxins and their role in grapevine trunk diseases. *Journal of Agricultural and Food Chemistry* 66:5948–5958
- Naidu RA, Perry EM, Pierce FJ, Mekuria T (2009) The potential of spectral reflectance technique for the detection of *Grapevine leafroll-associated virus* in two red-berried wine grape cultivars. *Computers and Electronics in Agriculture* 66:38–45
- Naidu RA, Rowhani A, Fuchs M, Golino D, Martelli GP (2014) Grapevine leafroll: a complex viral disease affecting a high-value fruit crop. *Plant Disease* 98:1172–1185
- Naidu RA, Maree HJ, Burger JT (2015) Grapevine leafroll disease and associated viruses: a unique pathosystem. *Annual Review of Phytopathology* 53:613–634
- Oerke EC, Herzog K, Toepfer R (2016) Hyperspectral phenotyping of the reaction of grapevine genotypes to *Plasmopara viticola*. *Journal of Experiment Botany* 67:5529–5543
- Osman F, Leutenegger C, Golino D, Rowhani A (2007) Real-time RT-PCR (TaqMan) assays for the detection of *Grapevine leafroll associated viruses* 1-5 and 9. *Journal of Virological Methods* 141:22–29
- Pérez-Roncal C, López-Maestresalas A, López-Molina C, Járen C, Urrestarazu J, Santesteban LG, Arazuri S (2020) Hyperspectral imaging to assess the presence of powdery mildew (*Erysiphe necator*) in cv. Carignan Noir grapevine bunches. *Agronomy* 10:88
- Petit AN, Vaillant N, Boulay M, Clement C, Fontaine F (2006) Alteration of photosynthesis in grapevines affected by esca. *Phytopathology* 96:1060–1066
- Poblete T, Camino C, Beck PSA, Homero A, Kattenborn T, Saponari M, Boscia D, Navas-Cortes JA, Zarco-Tejada PJ (2020) Detection of *Xylella fastidiosa* infection symptoms with airborne multispectral and thermal imagery: assessing bandset reduction performance from hyperspectral analysis. *ISPRS Journal of Photogrammetry and Remote Sensing* 162:27–40
- Prabhakar M, Prasad YG, Rao MN (2012) Remote sensing of biotic stress in crop plants and its applications for pest management. In: Venkateswarlu B, Shanker AK, Shanker C, Maheswari M (eds) *Crop stress and its management: perspectives and strategies*. Springer, New York, pp 517–549
- Reveglia P, Masi M, Cimmino A, Michereff S, Cinelli T, Mugnai L, Evidente A (2019) Phytotoxins produced by *Lasioidiplodia laeliocattleyae* involved in Botryosphaeria dieback of grapevines in Brazil. *Phytopathologia Mediterranea* 58:207–211
- Rohart F, Gautier B, Singh A, Lê Cao K-A (2017) mixOmics: an R package for ‘omics feature selection and multiple data integration. *PLoS Computational Biology* 13:e1005752
- Rott ME, Jelkmann W (2001) Characterization and detection of several filamentous viruses of cherry: adaptation of an alternative cloning method (DOP-PCR) and modification of an RNA extraction protocol. *European Journal of Plant Pathology* 107:411–420
- Silva MA, Correia KC, Barbosa MAG, Câmara MPS, Gramaje D, Michereff SJ (2017) Characterization of Phaeoacremonium isolates associated with Petri disease of table grape in Northeastern Brazil, with description of Phaeoacremonium nordesticola sp. nov. *European Journal of Plant Pathology* 149:695–709
- Úrbez-Torres JR, Haag P, Bowen P, O’Gorman DT (2014) Grapevine trunk diseases in British Columbia: incidence and characterization of the fungal pathogens associated with Esca and petri diseases of grapevine. *Plant Disease* 98:469–482
- Valtaud CFC, Fleurat-Lessard P, Bourbouloux A (2009) Systemic effects on leaf glutathione metabolism and defence protein expression caused by esca infection in grapevines. *Function Plant Biology* 36:260–279
- Vanegas F, Bratanov D, Powell K, Weiss J, Gonzalez F (2018) A novel methodology for improving plant pest surveillance in vineyards and crops using uav-based hyperspectral and spatial data. *Sensors* 18:260
- Yan J-Y, Xie Y, Zhang W, Wang Y, Liu J-K, Hyde KD, Seem RC, Zhang G-Z, Wang Z-Y, Yao S-W, Bai X-J, Dissanayake AJ, Peng Y-L, Li X-H (2013) Species of Botryosphaeriaceae involved in grapevine dieback in China. *Fungal Diversity* 61:221–236
- Yang T, Groenewald JZ, Cheewangkoon R, Jami F, Abdollahzadeh J, Lombard L, Crous PW (2017) Families, genera, and species of Botryosphaeriales. *Fungal Biology* 121:322–346
- Zarco-Tejada PJ, Camino C, Beck PSA, Calderon R, Homero A, Hernández-Clemente R, Kattenborn T, Montes-Borrego M, Susca L, Morelli M, Gonzalez-Dugo V, North PRJ, Landa BB, Boscia D, Saponari M, Navas-Cortes JA (2018) Pre-visual symptoms of *Xylella fastidiosa* infection revealed in spectral plant-trait alterations. *Nature Plants* 4:432–439
- Zhang M, Liu X, O’neil M (2002) Spectral discrimination of *Phytophthora infestans* infection on tomatoes based on principal component and cluster analyses. *International Journal of Remote Sensing* 23:1095–1107

**Publisher’s note** Springer Nature remains neutral with regard to jurisdictional claims in published maps and institutional affiliations.